Available online at www.sciencedirect.com
ScienceDirect
Proceedings of the Combustion Institute 31 (2007) 2473–2480
Proceedings of the Combustion Institute
www.elsevier.com/locate/proci

Cell-like structure of unstable oblique detonation wave from high-resolution numerical simulation ☆

Jeong-Yeol Choi [a,*], Dong-Wan Kim [a], In-Seuck Jeung [b], Fuhua Ma [c], Vigor Yang [c]

[a] *Pusan National University, Busan 609-735, Republic of Korea*
[b] *Seoul National University, Seoul 151-742, Republic of Korea*
[c] *Pennsylvania State University, University Park, PA 16802, USA*

Abstract

A comprehensive numerical study was carried out to investigate the unsteady cell-like structures of oblique detonation waves (ODWs) for a fixed Mach 7 inlet flow over a wedge of 30° turning angle. The effects of grid resolution and activation energy were examined systematically at a dimensionless heat addition of 10. The ODW front remains stable for a low activation energy regardless of grid resolution, but becomes unstable for a high activation energy featuring a cell-like wave front structure. Similar to the situation with an ordinary normal detonation wave (NDW), a continuous increase in the activation energy eventually causes the wave-front oscillation to transit from a regular to an irregular pattern. The wave structure of an unstable ODW, however, differs considerably from that of a NDW. Under the present flow condition, triple points and transverse waves propagate downstream, and the numerical smoke-foil record exhibits traces of triple points that rarely intersect with each other. Several instability-driving mechanisms were conjectured from the highly refined results. Since the reaction front behind a shock wave can be easily destabilized by disturbance inherent in the flowfield, the ODW front becomes unstable and displays cell-like structures due to the local pressure oscillations and/or the reflected shock waves originating from the triple points. The combined effects of various instability sources give rise to a highly unstable and complex flow structure behind an unstable ODW front.
© 2006 The Combustion Institute. Published by Elsevier Inc. All rights reserved.

Keywords: Oblique detonation wave; Unstable detonation; Cell structure; Numerical simulation

1. Introduction

Oblique detonation waves (ODWs) stabilized over inclined walls have long been considered as a promising combustion means for hypersonic propulsion systems such as ODW engines and ram accelerators. A number of studies were carried out to examine the fundamental characteristics of an ODW and its implementation for propulsion systems. Pratt et al. [1] applied classical detonation theories by assuming immediate heat addition behind an oblique shock wave (OSW). Shepherd [2] reported the state of knowledge about ODW for propulsion applications as of 1994. The ODW phenomena has been observed by using the two-layer detonation tubes for

☆ Supplementary data for this article can be accessed online. See Appendix A.

* Corresponding author. Fax: +82 51 513 3760.
E-mail address: aerochoi@pusan.ac.kr (J.-Y. Choi).

1540-7489/$ - see front matter © 2006 The Combustion Institute. Published by Elsevier Inc. All rights reserved.
doi:10.1016/j.proci.2006.07.173

two-dimensional configurations [3,4] and the ballistic range facilities for axi-symmetric configurations [5–7]. Morris et al. [8] employed an expansion tube to study oblique-shock-induced combustion. These experimental works have provided much insight into the ODW dynamics and structures.

The structure of a stable ODW was first studied numerically by Li et al. [9]. Results revealed the wave behaviors in various regimes, depending on specific flow parameters of concern. Thaker and Chelliah [10] examined the hydrogen combustion for ODW using both detailed and reduced chemical reaction mechanisms. Papalexandris [11] investigated the regimes and stabilities of ODWs for infinite- and finite-length wedges by considering a one-step chemical reaction. The instability of an ODW front involving multiple triple points was demonstrated. Figueira da Silva and Deshaies [12] studied the transition from an oblique-shock to an oblique-detonation wave as a function of various flow parameters. Fusina et al. [13] investigated the stability of a detonation wave and found that the wave is resilient to inflow perturbations, a phenomenon similar to that previously reported by Li et al. [9].

Most of experiments revealed a preheat zone behind an OSW and some of them showed transverse waves behind an ODW [3,4]. The latter were believed to produce cellular structures in a manner to those associated with a normal detonation wave. Papalexandris [11] numerically explored the instability of an ODW front. Detailed investigations on the cell structures, however, are not currently available for unstable ODW front structures, because of obstacles arising from the significant difference in the induction length behind an OSW and an ODW. High-resolution observation of ODW front structures was difficult in experiments, although some measurable induction distances behind OSWs have been obtained. In numerical simulations, the stringent grid-resolution requirement for a wide computational domain covering the preheat zone behind a shock wave prohibits high-fidelity simulations of ODW front structures. The present study attempts to circumvent these limitations by conducting a thorough investigation into the unstable structure of an ODW front at a scale sufficient to provide detailed information not available in the existing literature.

2. Theoretical formulation and numerical method

Because of the daunting requirement for numerical grid resolution in the present study, a simple, yet realistic, formulation is employed. The analysis is based on the Euler equations for an inviscid compressible flow, and takes into account the conservation of a reaction-progress variable. The governing equations in a two-dimensional coordinate system can be summarized in the following vector form:

$$\frac{\partial}{\partial t}\begin{bmatrix}\rho\\ \rho u\\ \rho v\\ \rho e\\ \rho Z\end{bmatrix}+\frac{\partial}{\partial x}\begin{bmatrix}\rho u\\ \rho u^2+p\\ \rho uv\\ (\rho e+p)u\\ \rho Zu\end{bmatrix}+\frac{\partial}{\partial y}\begin{bmatrix}\rho v\\ \rho uv\\ \rho v^2+p\\ (\rho e+p)v\\ \rho Zv\end{bmatrix}=\begin{bmatrix}0\\ 0\\ 0\\ 0\\ \rho w\end{bmatrix}, \tag{1}$$

where the pressure is obtained through the equation of state

$$p=(\gamma-1)\rho\left\{e-\frac{1}{2}(u^2+v^2)+Zq\right\}. \tag{2}$$

The reaction-progress variable, Z, characterizes the mass fraction of product species, and varies between 0 and 1. The dimensionless heat addition is denoted by q. A one-step Arrhenius-type reaction model is used to simulate the various regimes of detonation phenomena without the complexity and large computing time associated with multiple chemical species and reaction steps. The reaction rate in Eq. (1) thus depends only on the mixture concentration as follows:

$$w=(1-Z)k\exp(-E_a\rho/p), \tag{3}$$

where k is the pre-exponential factor and E_a the activation energy. The conservation equations are discretized by means of a finite-volume formulation. The convective fluxes are calculated by Roe's approximate Riemann solver, with the primitive variables interpolated by a third-order accurate MUSCL-type TVD scheme. The discretized equations are integrated in time using a fourth-order accurate, four-stage Runge–Kutta scheme. Details about the theoretical formulation and numerical algorithms are given in Refs. [14,15].

3. Simulation conditions

Since severe numerical difficulties in capturing the cell-like ODW front structure may arise from the significant difference between the induction lengths behind a shock and a detonation wave, a judicious selection of simulated flow conditions must be made to reduce the disparity of induction length. In the present study, a Mach 7 flow with a specific heat ratio of $\gamma=1.3$ over a 30° wedge is treated, as shown schematically in Fig. 1. A relatively small value of 10.0 is assumed for the dimensionless heat addition, q, to render the difference between the OSW and ODW angles to a range that can be managed computationally. The resultant wave angles are 37.6° for the OSW and 48.6° for the ODW. A rectangular computational domain is considered over the wedge with

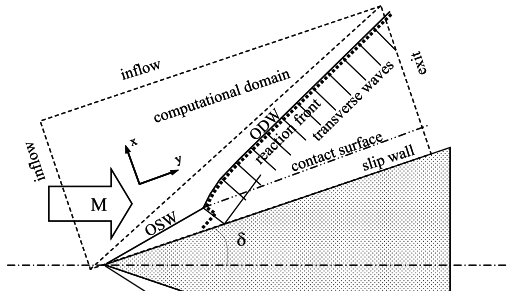

Fig. 1. Schematics of flow configurations and coordinate system.

a dimensionless size of 1.0×0.4, and a wedge-surface attached coordinate system is employed. The flow enters the computational domain at the flow turning angle, as did in the previous studies [9–13]. Five different levels of numerical grid resolution (i.e., 255×100, 505×200, 1005×400, 2005×800 and 4005×1600) are considered. The corresponding grid sizes are $\Delta x = \Delta y = 1/250$, $1/500$, $1/1000$, $1/2000$ and $1/4000$, respectively. Five additional cells are added upstream of the wedge surface to avoid any numerical reflection from the left boundary. Slip boundary conditions are used at the wedge surface. The inlet boundary conditions are fixed at the prespecified values, and the flow properties at the exit are extrapolated from the interior.

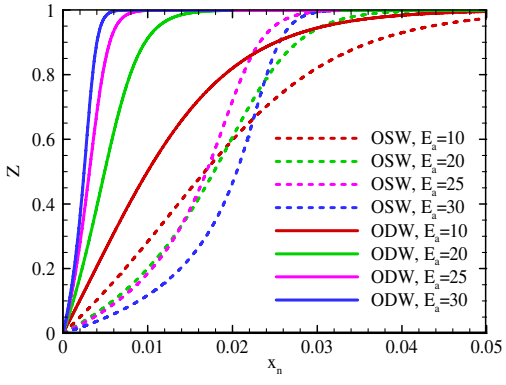

Fig. 2. Effect of activation energy on the distribution of reaction progress variable along the wave normal direction. Obtained from the calculated ZND structure behind OSW and ODW.

To study the influence of activation energy on the wave instability characteristics, different values of $E_a = 10$, 20, 25 and 30 were considered. The pre-exponential factor, k, is adjusted to capture the primary triple point over the wedge surface at the dimensionless distance of $x \approx 0.2$. As a first step in the numerical simulation, the ZND structures were calculated by using the flow conditions behind the OSW and ODW to estimate the grid requirement, in a manner similar to the NDW simulations in our previous study [14]. Figure 2 shows the distribution of the reaction progress variable along the wave normal direction behind the OSW and ODW from the steady ZND calculations. Table 1 lists the adjusted pre-exponential factors and half-reaction lengths, $L_{1/2}$, which measure the normal distances behind the waves by neglecting the wave tangential velocity component. A higher activation energy leads to a higher ratio of $L_{1/2}^{OSW}$ to $L_{1/2}^{ODW}$, suggesting a more refined grid is required to capture the ZND structure behind the ODW. For example, the finest grid of 4005×1600 considered in the present study has 10 grid cells within $L_{1/2}$ behind the ODW for the extreme case of $E_a = 30$, and around 80 grid cells behind the OSW along the wave normal direction. But in practice, a vast number of grid cells could be included between the shock wave and reaction front in the flow direction, due to the presence of the wave tangential velocity that may be several times larger than its normal counterpart.

4. Results and discussion

4.1. Stable ODW with low activation energy

Figure 3a shows a calculated snapshot of the temperature field for the case of $E_a = 10$ with the 2005×800 grid. No coupling between the shock and reaction front occurs, and the OSW transits to the ODW very smoothly. Figure 3b

Table 1
Pre-exponential factor, half-reaction-zone length, and dimensionless activation energy behind OSW and ODW

	$E_a = 10$	$E_a = 20$	$E_a = 25$	$E_a = 30$
k	5×10^2	1×10^4	5×10^4	2×10^5
$L_{1/2}^{OSW}$	1.67×10^{-2}	1.78×10^{-2}	1.62×10^{-2}	2.05×10^{-2}
$L_{1/2}^{ODW}$	9.98×10^{-3}	4.92×10^{-3}	3.12×10^{-3}	2.49×10^{-3}
$L_{1/2}^{OSW}/L_{1/2}^{ODW}$	1.67	3.62	5.19	8.23
θ_{OSW}	2.72	5.43	6.79	8.14
θ_{ODW}	1.99	3.98	4.97	5.97

Dimensionless activation energy $\theta = E_a/T_{VN}$.

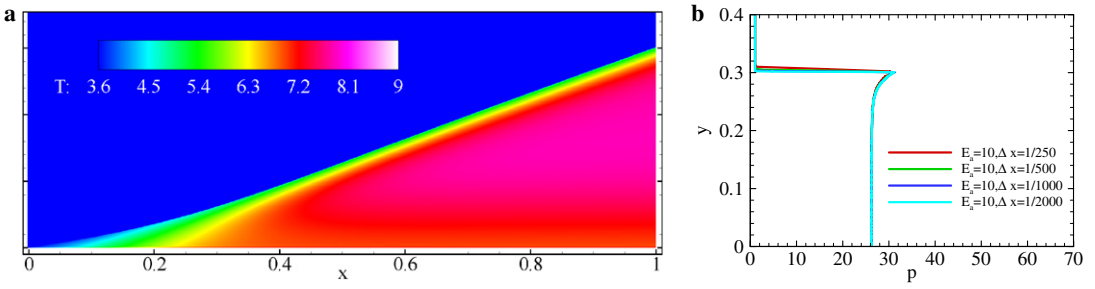

Fig. 3. Stable ODW for the case of $E_a = 10$, (a) snapshot of temperature field with $\Delta x = 1/2000$, (b) exit pressure profiles with different grids.

compares the pressure profiles at the exit of the computational domain with different grid resolutions. All the results coincide to a single distribution. The residual error of the calculated density field for each grid system is less than 10^{-4}. Thus, the case of $E_a = 10$ is considered as a stable ODW without any oscillations at the wave front. The calculated OSW and ODW angles are 38° and 49°, respectively, agreeing well with the theoretical values of 37.6° and 48.6°.

Figure 4a shows the results for the case of $E_a = 20$ based on the 2005×800 grid. The coupling between the shock wave and reaction front is clearly observed, although the interaction is not strong enough and the OSW smoothly transits to a detonation wave. The exit pressure profiles shown in Fig. 4b indicate a stronger pressure spike than that in the case of $E_a = 10$. The phenomenon may be attributed to the narrower ZND structure with increasing E_a, as evidenced by $L_{1/2}^{ODW}$ in Table 1. The results with different grids agree well with each other and the numerical-convergence characteristics are similar to those for $E_a = 10$. Therefore, the case of $E_a = 20$ is also considered as a stable ODW. It is worth noting that those stable ODWs with low activation energies have not been observed in experiments, and must be treated as theoretically limiting cases.

4.2. Regularly unstable ODW with moderate activation energy, $E_a = 25$

Figures 5a–d show the calculated snapshots of temperature field for $E_a = 25$ with four different grid resolutions. The coarsest grid size is greater than $L_{1/2}^{ODW}$, and the finest grid gives six grid cells within $L_{1/2}^{ODW}$. The wave front associated with the 255×100 grid is quite smooth. Instability starts to take place with the 505×200 grid, as revealed by the variation of the wave-front thickness in Fig. 5b. The situation becomes much more obvious for the 1005×400 grid, especially in the region near the end of the computational domain shown in Fig. 5c. A shock wave, generated at the primary triple point and reflected from the wedge surface, passes across the slip surface and interacts with the ODW. It is generally believed that the instability at the wave front grows out of reinforcement between the disturbances inherent in the flowfield and shock waves. A small disturbance initially produced by numerical errors propagates downstream along the wave tangential direction and then amplifies to interact with the ODW structure.

Figure 5d shows the result with the 2005×800 grid. The ODW front instability is clearly observed with well-organized cell-like structures. A close-up view is given in Fig. 6, along with a

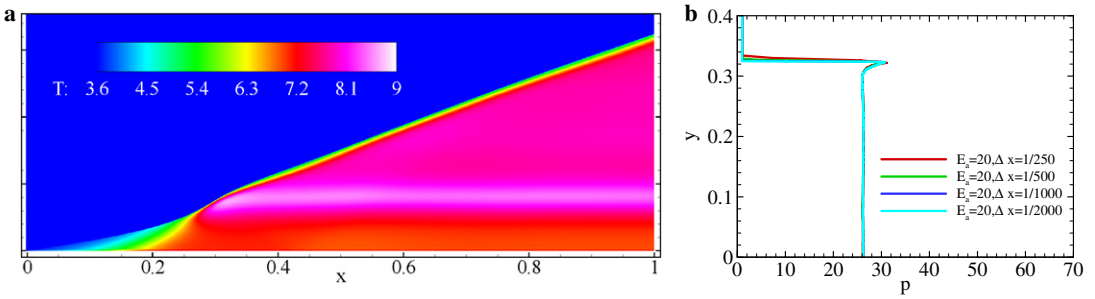

Fig. 4. Stable ODW for the case of $E_a = 20$, (a) snapshot of temperature field with $\Delta x = 1/2000$, (b) exit pressure profiles with different grids.

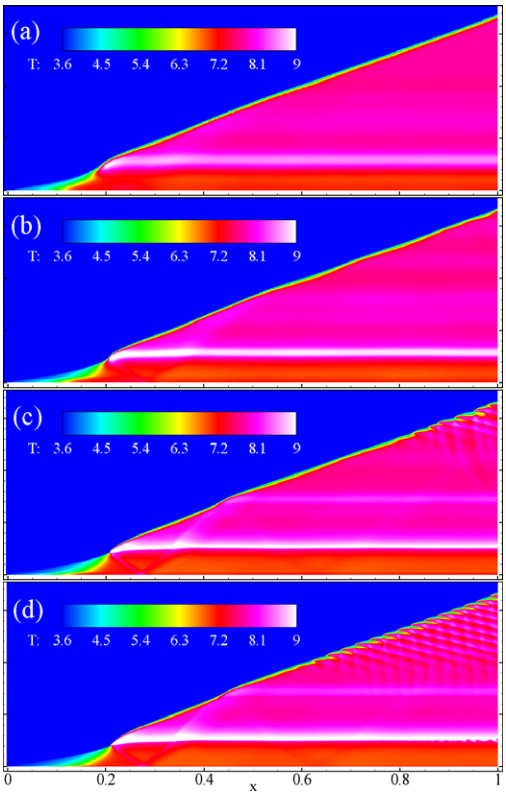

Fig. 5. Snapshots of temperature field for the case of $E_a = 25$ with different grids: (a) $\Delta x = 1/250$, (b) $\Delta x = 1/500$, (c) $\Delta x = 1/1000$, (d) $\Delta x = 1/2000$.

schematic diagram of the wave-front structure illustrating features distinct from those of a NDW front. Under current flow conditions, all the transverse waves propagate in the same direction behind the ODW. The situation bears a close resemblance to the numerically produced x–t diagram in Ref. [15] for Lehr's experiment of oscillating shock-induced combustion around a blunt body. The cell structure of an ordinary NDW may not be expected to occur for an unstable ODW on a smoke-foil record. Thus, we refer the unstable ODW front structure to a cell-like structure instead of a cell structure.

Figure 7a shows a more refined result with the 4005×1600 grid. The wave instability begins at a location where the reflected shock from the wall interacts with the ODW. Strong vorticity generation occurs at the slip surface originating from the primary triple point. The vortical field interacts with transverse waves from the unstable ODW front. The resultant reflected waves further interact with the ODW front. The highly refined numerical grid resolves many sources of flow disturbances that make the unstable ODW front irregular. Figure 7b shows instantaneous exit pressure profiles with different grids. A finer grid gives rise to stronger pressure unsteadiness. Nonetheless, all the calculations lead to the same ODW angle in the time-averaged sense, and agree well with the theoretical value of 48.6°.

4.3. Irregularly Unstable ODW with high activation energy, $E_a = 30$

Figure 8 shows calculated snapshots of temperature field for the case of $E_a = 30$ with four different grids. Flow unsteadiness is observed even with the coarsest 255×100 grid. A regular pattern of an unstable ODW structure is obtained with the 505×200 grid. A further refinement using the 1005×400 grid leads to an irregular pattern. The location where the unstable ODW structure begins at roughly the same position in Figs. 8b and c. An even finer resolution with the 2005×800 grid results in a very complex flow structure consisting of a strong vorticity generation mechanism from the primary triple point. The vortical field appears quite regular in this case. The unstable ODW structure starts to occur when the reflected shock wave interacts with the ODW front, though some instability phenomena are already present upstream of the interaction point. Also, a secondary vorticity is observed at the slip surface originating from the triple point of an unstable

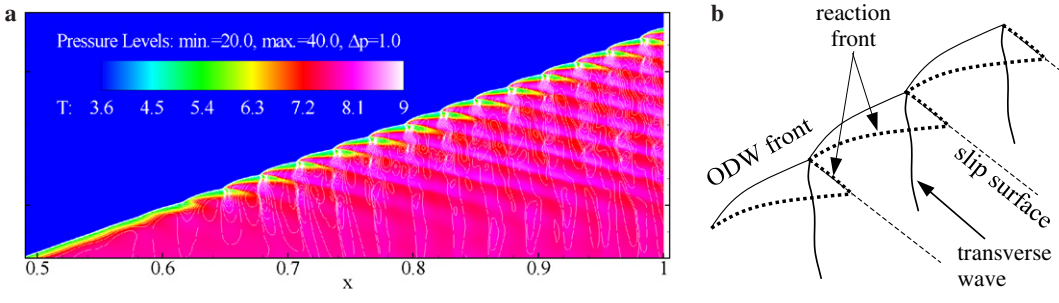

Fig. 6. Regularly unstable ODW front structure for the case of $E_a = 25$ with $\Delta x = 1/2000$, (a) close-up view of pressure and temperature fields, (b) schematic of wave front structure.

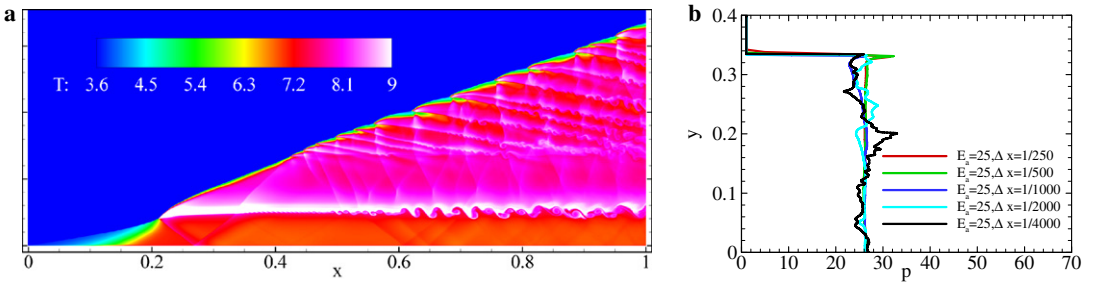

Fig. 7. Unstable ODW for the case of $E_a = 25$, (a) snapshot of temperature field with $\Delta x = 1/4000$, (b) exit pressure profiles with different grids.

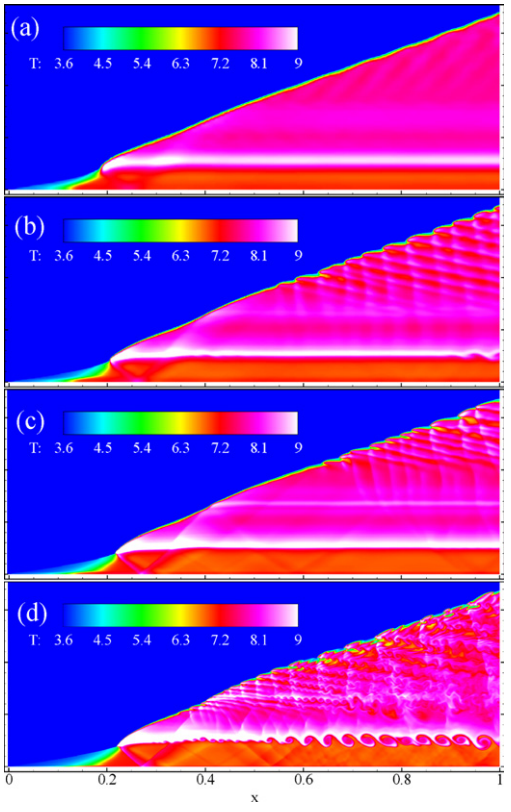

Fig. 8. Snapshots of temperature field for the case of $E_a = 30$, (a) $\Delta x = 1/250$, (b) $\Delta x = 1/500$, (c) $\Delta x = 1/1000$, (d) $\Delta x = 1/2000$.

ODW front. Figures 9a and b show the calculated pressure and temperature fields, respectively, using the 4005×1600 grid. The flow unsteadiness becomes quite strong, and the instability appears at a very early position around the primary triple point. As Viguier et al. observed in their experiment [4], the unstable ODW structure is small at the initial position and becomes larger as it moves downstream. The various sources of flow disturbances interact with each other, and consequently cause a complex flow structure. The flame front is disturbed accordingly and presents such an irregular wavy pattern. The exit pressure profiles shown in Fig. 9c indicate the irregularity of the pressure field. Although the flowfield behind the primary triple point is very complex, the preheat zone ahead of that point remains steady and nearly unchanged, as also demonstrated by the wall pressure distribution in Fig. 9d. The dominant peak in the wall pressure is caused by the reflected shock wave from the primary triple point. The calculated pressure profiles tend to converge as the grid becomes finer. The pressure distribution is relatively smooth upstream of the peak, but becomes oscillatory in the downstream region.

Figure 10 shows the numerical smoke-foil record for the 2005×800 grid, which is produced from the instantaneous maximum pressure along the ODW front in a rotated coordinate. The ODW front structure and triple-point traces can be clearly observed in this image. The angle of the triple-point trace is determined by the vector sum of the triple-point and flow velocities. As discussed before, no noticeable cell structure is observed because all transverse waves move in the same direction, although with slightly different speeds. The wiggles in the smoke foil result from the mis-alignment of the computational grid line with the flow direction. Figure 11 shows the pressure history at the location of $y = 3.0$ at the exit boundary, further demonstrating the unsteadiness of the wave structure. The contribution of various disturbances can be identified from a detailed analysis of the pressure history.

5. Conclusion

The effects of activation energy and numerical-grid resolution on unstable ODW structures were examined systematically. The ODW front remains stable for low activation energy regardless of the grid resolution. An increase in the activation ener-

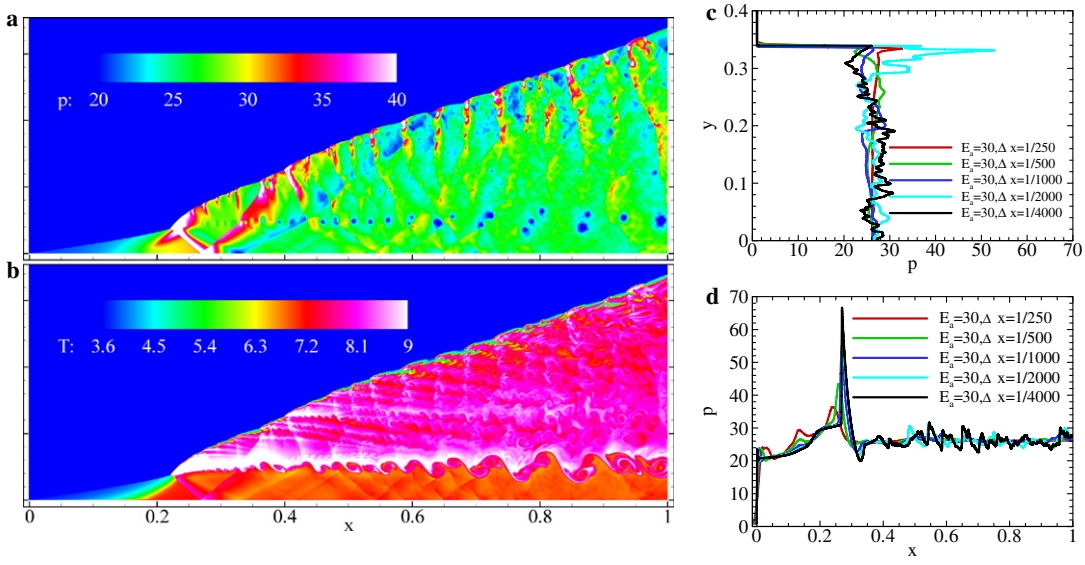

Fig. 9. Unstable ODW for the case of $E_a = 30$, (a) pressure field with $\Delta x = 1/4000$, (b) temperature field with $\Delta x = 1/4000$, (c) exit pressure profiles with different grids, (d) wall pressure profiles with different grids.

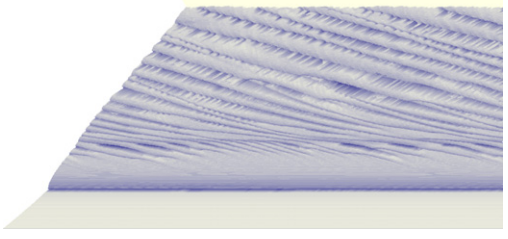

Fig. 10. Numerical smoke-foil record (maximum pressure trace) for the case of $E_a = 30$ with $\Delta x = 1/2000$.

gy may cause the wave front to exhibit cell-like structures, which then transit from a regular to an irregular pattern as the activation energy further increases. The phenomenon bears a qualitative resemblance to that for a NDW. The activation energy, however, exerts little influence on the mean wave angles of the OSW and ODW. They both agree well with their respective theoretical values.

The wave structure of an unstable ODW possesses features distinct from those of a NDW. Under the present flow conditions, the triple points and transverse waves propagate only downstream. The numerical smoke-foil record displays triple-point traces that rarely intersect with each other. Several sources of instabilities were examined for the highly unstable cases. The ODW front becomes unstable and displays cell-like structures due to the local pressure oscillations and/or the reflected shock waves originating from the triple points. The combined effects of various instability sources give rise to a highly unstable and complex flow structure behind an unstable ODW front.

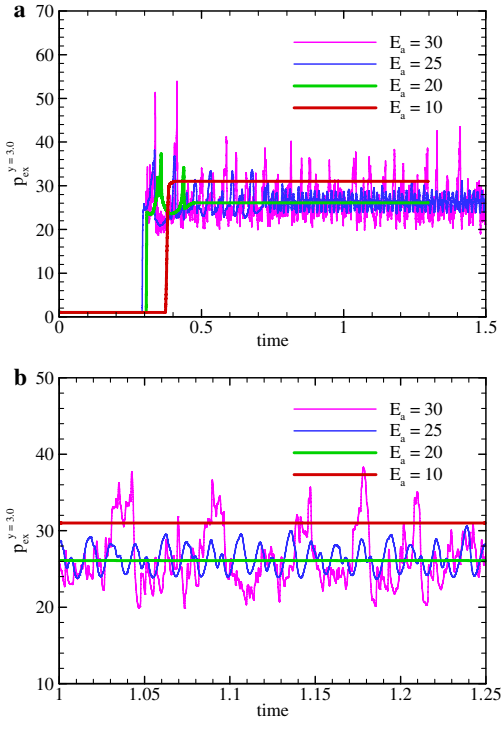

Fig. 11. Exit pressure variations at $y = 3.0$, (a) time history over the entire computation, (b) close-up view.

Acknowledgments

Present work has been sponsored partly by the Korea Research Foundation Grant funded by the Korean Government (MOEHRD) (KRF-2006-521-D00061), and the National Research Laboratory program (M10500000072-05J000007210) of Korea Science and Engineering Foundation.

Appendix A. Supplementary data

Supplementary data associated with this article can be found in the online version at doi:10.1016/j.proci.2006.07.173.

References

[1] D.T. Pratt, J.W. Humphrey, D.E. Glenn, *J. Prop. Pow.* 7 (5) (1991) 837–845.
[2] J.E. Shepherd, in: J. Buckmaster, T.L. Jackson, A. Kumar (Eds.), *Combustion in High-Speed Flows*, Kluwer, Dordrecht, 1994, p. 373.
[3] E.K. Dabora, D. Desbordes, C. Guerraud, H.G. Wagner, *Prog. Aero. Astro.* 133 (1991) 187–204.
[4] C. Viguier, A. Gourara, D. Desbordes, B. Deshaies, *Proc. Combust. Inst.* 27 (1998) 2207–2214.
[5] H.F. Lehr, *Astronautica Acta* 17 (1972) 589–597.
[6] M.J. Kaneshige, J.E. Shepherd, *Proc. Combust. Inst.* 26 (1996) 3015–3022.
[7] J. Kasahara, T. Fujiwara, T. Endo, T. Arai, *AIAA J.* 39 (2001) 1553–1561.
[8] C.I. Morris, M.R. Kamel, R.K. Hanson, *Proc. Combust. Inst.* 27 (1998) 2157–2164.
[9] C. Li, K. Kailasanath, E.S. Oran, *Phys. Fluids* 6 (4) (1994) 1600–1611.
[10] A.A. Thaker, H.K. Chelliah, *Combust. Theory Modeling* 1 (1997) 347–376.
[11] M.V. Papalexandris, *Combust. Flame* 120 (2000) 526–538.
[12] L.F. Figueira da Silva, B. Deshaies, *Combust. Flame* 121 (2000) 152–166.
[13] G. Fusina, J.P. Sislian, B. Parent, *AIAA J.* 43 (7) (2005) 1591–1604.
[14] J.-Y. Choi, F.H. Ma, V. Yang, *AIAA Paper* (2005) 1174–2005.
[15] J.-Y. Choi, I.-S. Jeung, Y.Y. Yoon, *AIAA J.* 38 (7) (2000) 1179–1187.

Comment

Luc Bauwens, University of Calgary, Canada. In your conclusions, you explain that transverse waves only move in one direction, in contrast with planar detonations, because the flow downstream is subsonic. But surely, in a frame of reference in which the incoming supersonic un-burnt flow is normal to the shock, the flow behind the shock is subsonic? So, I would think that you obtain one set of waves from the origin, at the bottom left of your pictures, but the reason for the absence of a second set is that the first set never has a surface on which to reflect?

Reply. Since the flow regime is the overdriven oblique detonation wave, the flow speed behind the shock wave is supersonic. What I meant in the presentation is that only the normal speed component is subsonic if we split the flow speed into wave normal and tangential components. It is already discussed in the manuscript and the first question may come from the misunderstanding. Though not included in the manuscript but presented at the end of my talk, further study on this topic reveals that the dual set of transverse waves propagating in opposite directions are only observed for the very special condition at the maximum flow turning angle of oblique detonation wave at the detonation polar diagram, where the flow speed behind ODW is very close to the speed of sound. At this condition, the set of transverse waves is initiated by the intrinsic wave instability rather than the wave reflections. Thus, the inference that the reason for the absence of a second set is that the first set never has a surface on which to reflect is partly true, but may not be a fundamental explanation.